Supplementary Materials for

Actin Network Architecture Can Determine Myosin Motor Activity

Anne-Cécile Reymann[1], Rajaa Boujemaa-Paterski[1], Jean-Louis Martiel[1], Christophe Guérin[1], Wenxiang Cao[2], Harvey F. Chin[2], Enrique M. De La Cruz[2], Manuel Théry[1*] & Laurent Blanchoin[1*].

*To whom correspondence should be addressed.
E-mail: manuel.thery@cea.fr, laurent.blanchoin@cea.fr

This PDF file includes:

Materials and Methods
Figs. S1 to S9
Captions for Movies S1 to S11

Other Suplementary Materials for this manuscript includes the following:

Movies S1 to S11

Materials and Methods

Protein expression and purification

Actin was purified from rabbit skeletal-muscle acetone powder. Actin was labeled on lysines with Alexa-568 according to Isambert and colleagues (*16*). Arp2/3 complex was purified from bovine brain extracts as according to Egile and colleagues (*17*). GST-pWA and human profilin were expressed and purified as described previously. Double-headed (referred to as HMM) porcine myosin VI with bound calmodulin was purified from Sf9 cells by FLAG affinity chromatography (*12*, *18*). Muscle myosin was purified from rabbit skeletal muscle according to (*19*).

Micropatterning

Micropatterning of Nucleating Promoting Factor pWA was performed either with substrate exposure to deep-UV through a photomask (*11*) or with substrate scanning with a pulsed UV laser (*20*). Multipatterning for pWA and myosinVI on two separate regions (Fig. S5) were made following the deep-UV based protocol of surface modification. After the grafting of pWA on a first set of micropatterns, coverslips were dried, exposed again to deep UV light through a quartz photomask, mounted in flow cells with adhesive double tape and coated successively with G protein (0.5 mg/mL), GFP-antibodies (160 µg/mL), BSA (5% w/v) and GFP-HMM-myosin VI (80 nM).

Actin polymerization

Actin polymerization was induced in a solution containing 2 µM actin monomers (7% labelled with Alexa-568), 6 µM profilin, 30 nM Arp2/3 complex and when not specified, 8 nM of HMM-myosin VI (GFP labelled) or 160 nM of muscle myosin II. These proteins mixture were diluted in freshly prepared buffer containing 15 mM imidazole-HCl (pH 7.8), 0.6 mM ATP, 55 mM DTT, 1 mM EGTA, 75 mM KCl, 3.5 mM $MgCl_2$, 1.5 mg/mL glucose, 10 µg/mL catalase, 50 µg/mL glucose oxidase, and 0.25 % w/v methyl-cellulose. An ATP regenerator system was also added to this medium (2 mM MgATP, 2 mM phosphoenolpyruvate, 2000 U/mL pyruvate kinase).

Image acquisition

Images were taken using a straight BX61 Olympus microscope equipped with a 40x dry objective (UPLFLN, NA=0,75), an XY motorized stage (Marzhauser, Germany) and a CoolSnap HQ2 camera (Roper Scientific, GmbH, Germany). Microscope and devices were driven by MetaMorph (Molecular Devices, Downington, PA).

Image treatment and analysis

All set of images were taken using the same light intensity and exposure time. However, before being displayed, images grey scales were adjusted to have the same minimum and maximum grey values. Fluorescence analysis (linescans of fluorescent intensities and kymographs) was performed using ImageJ toolboxes.

Semi-automated analysis of data of ring contraction rates

A specific semi-automated analysis of data was developed using ImageJ (*21*) and Matlab for the analysis of myosin induced-contraction of actin networks on patterned rings (Fig. 3). Myosin induced constricting rings were first analyzed with ImageJ either manually (for dotted rings) or using the 2D JFilament plugins (for regular rings) to obtain the precise position of the denser actin gel as it constricts. These continuous contours obtained for full rings were divided in small angular sectors using the instantaneous center of the actin structure. For dotted rings, angular sectors were defined by the distance in between two dots of branched meshwork. Data were analyzed using a Matlab program enabling the automated measuring of network deformation by the analysis of the constriction rate of all sectors of rings. Linear approximations were made to distinguish the different phases of movement (lag, rapid decrease and slow decrease) and determine the precise time point, t0, corresponding to the beginning of the fast phase (linear phase with the maximum constriction velocity). For comparisons between different patterns and evaluation of proportions or means all curves were time shifted to zero at t0 in order to numerically synchronize the beginning of sector contraction. Each contraction curve then adopted the same profile. Average velocity values were reported in figures 3 and 4. Errors bars indicated standard errors. Statistical comparisons were Student tests, *** = $P<0.001$, ns = no significant difference = $P > 0.05$.

Analysis of fluorescence intensities during ring contraction

Fluorescence intensities were measured on the previously defined angular sectors. Intensities were normalized with respect to the value measured at the beginning of network deformation, which was considered as the time origin. The distinct experiments were numerically shifted in time to have the same time origin. Normalized intensity values were averaged over several experiments. Statistical comparisons in fig. S8 were Student tests, *** = $P<0.001$, ns = no significant difference = $P > 0.05$.

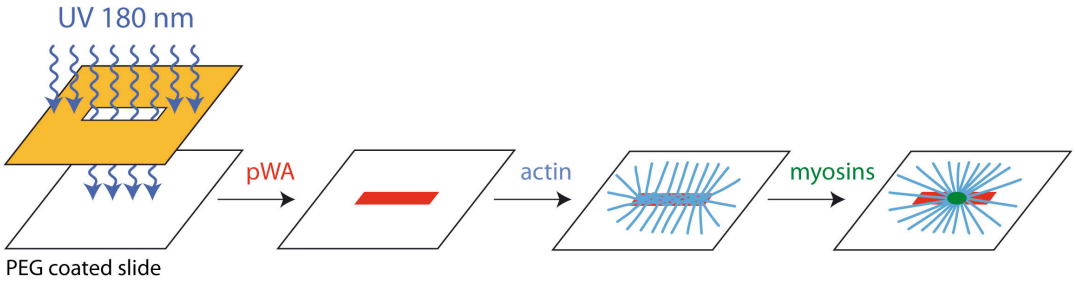

Fig. S1. Surface-micropatterning method.

Deep UV exposure through a photomask creates micropatterns on poly-ethyleneglycol coated glass slide (*11*). The micropatterned slide is incubated with WASp-PWA to adsorb on the micropatterned regions. In the presence of the actin polymerizing mix and myosins, filaments should grow on and out of the micropattern and get contracted.

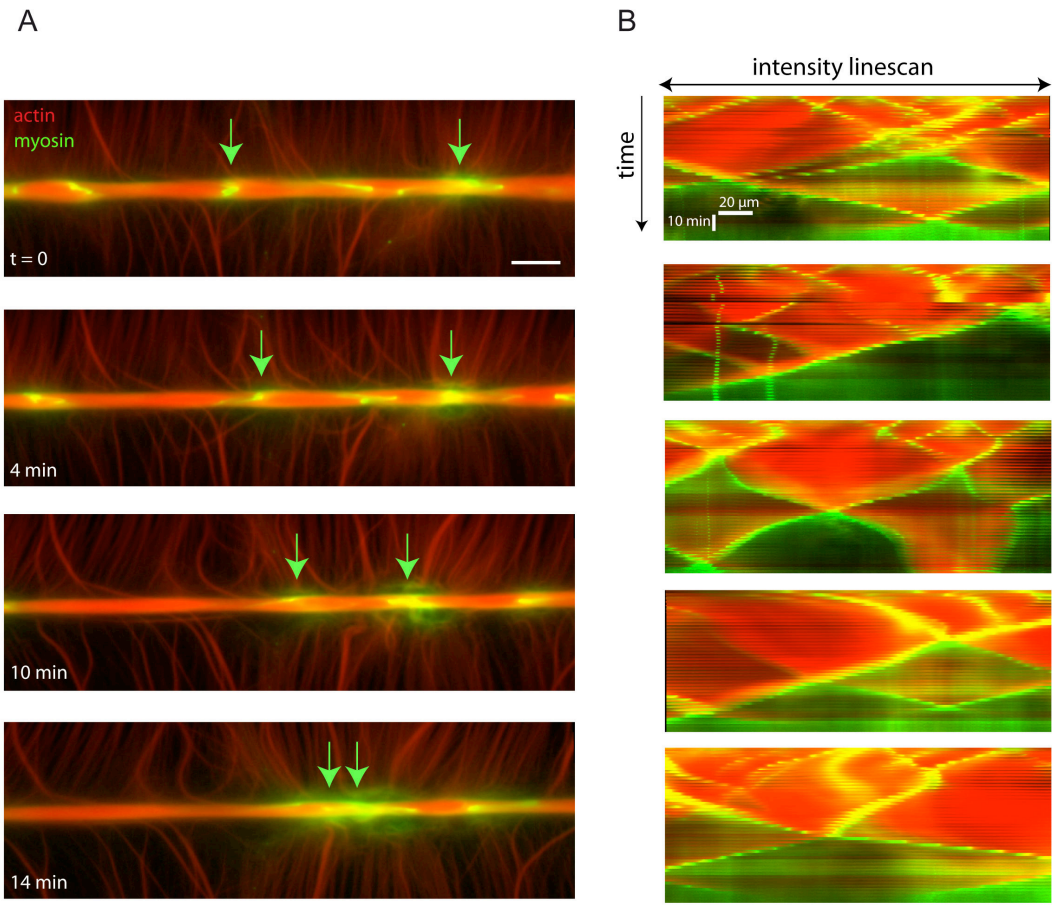

Fig. S2. Myosin induced actin meshwork contraction and disassembly.

(A, B) Time-series of the myosin VI-induced deformation of the actin meshwork nucleated on long PWA-coated bars. Actin is shown in red, myosin VI in green. **(A)** Parallel filaments growing out of the nucleation bar remained unaffected, while the branched meshwork on the bar did contract. Accumulation of myosin-VI (green arrows) was coupled to local network disassembly. As the network disassembles, these myosin-rich spots moved along the meshwork (see green arrows displacements). Scale bar is 20 µm. **(B)** Kymographs were obtained by doing fluorescence intensity linescans along the meshwork every two minutes for 6 distinct bars. They highlight the displacements of myosin-rich spot (green) and the associated network disassembly (red fluorescence decrease). Disassembly wave velocities, as revealed by myosin-rich densities displacements, appeared to be distributed around 1 micron per minute.

The disassembly process can either follow network deformation (as the short bars of fig. 1 and movie S2) or propagate on a non-deforming network (as these long bars and reticulated networks of movie S4). On short bars the distal parts are submitted to asymmetric force distribution, they detach and get deformed. The network collapses at the bar center where it get disassembled (Fig. 1 and movie S2). On these long bars the central part, which is shown in the figure, remains attached and induces the formation of a disassembly wave (Fig. S2).

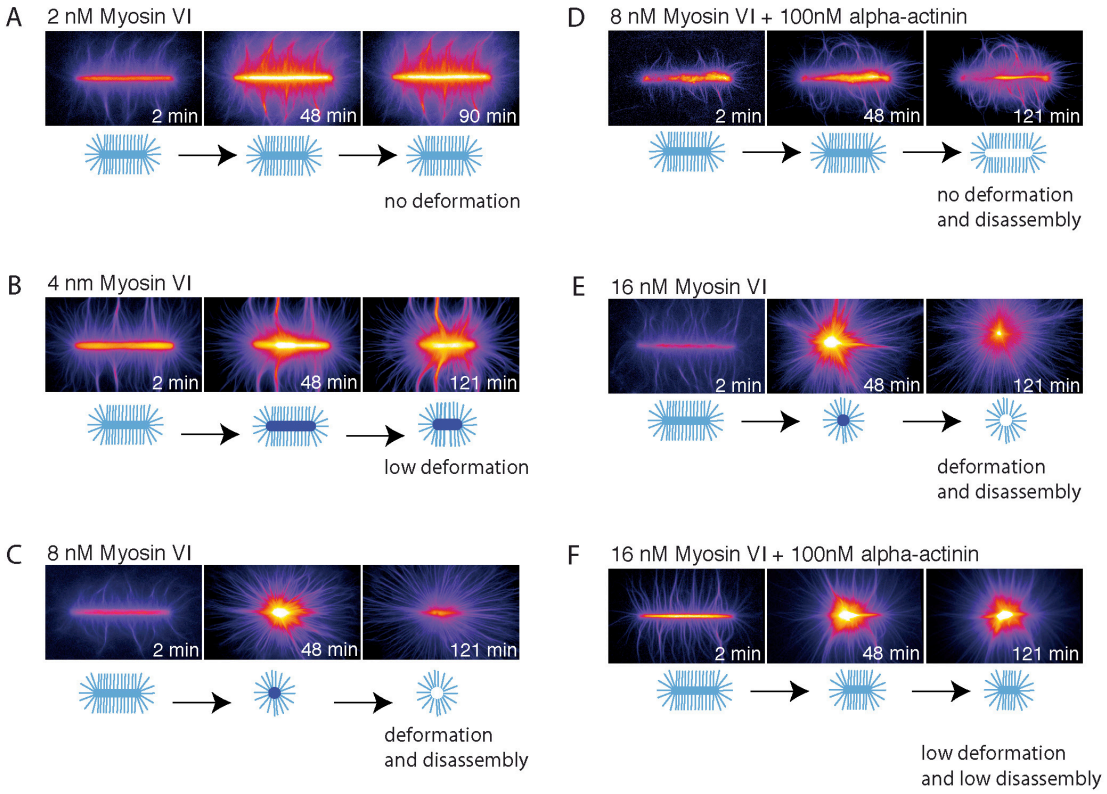

Fig. S3. **Myosin concentration determines actin contraction dynamics.**

90-microns long bars were used to induced the formation of controlled and reproducible actin networks with a dense meshwork of branched filaments on the bar and parallel arrays of filament out of the bar. Various concentrations of myosin VI were added to the polymerization mix. Low concentration of myosin (2 nM) did not induce network deformation or disassembly. Higher concentrations (4 nM) induced network deformation but not disassembly. Above a critical concentration (8 nM) the networks were both deformed and disassembled. Addition of the actin crosslinker alpha-actinin modulates the effect of myosin.

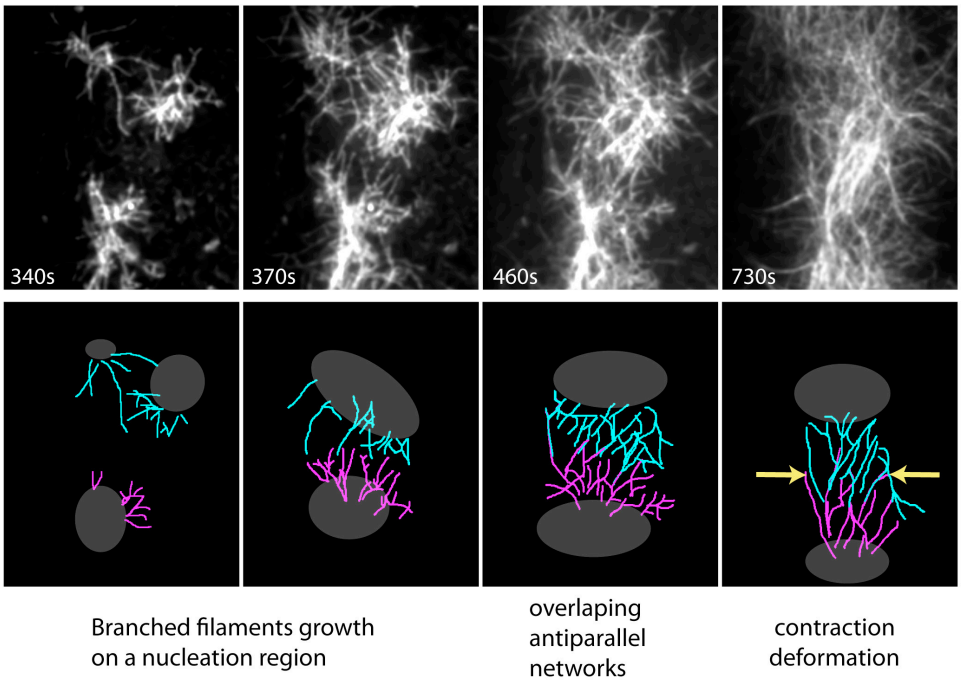

Fig. S4. **Anti-parallel filament overlapping triggers network contraction and deformation.**

Branched filaments were initiated on a large bar homogeneously coated with pWA by adding an actin polymerization mix including a low concentration of Arp2/3 (10 nM). Individual filament growth was monitored with TIRF microscopy. Although myosin VI is present in the mix, neither alignment of filament nor contraction of the network could be observed as long as the distinct networks remained separated (first two images). Once the networks contact each other (third image) their filaments formed anti-parallel associations. The action of myosins on these anti-parallel bundles led to filament alignment, bundle contraction and network deformation (fourth image).

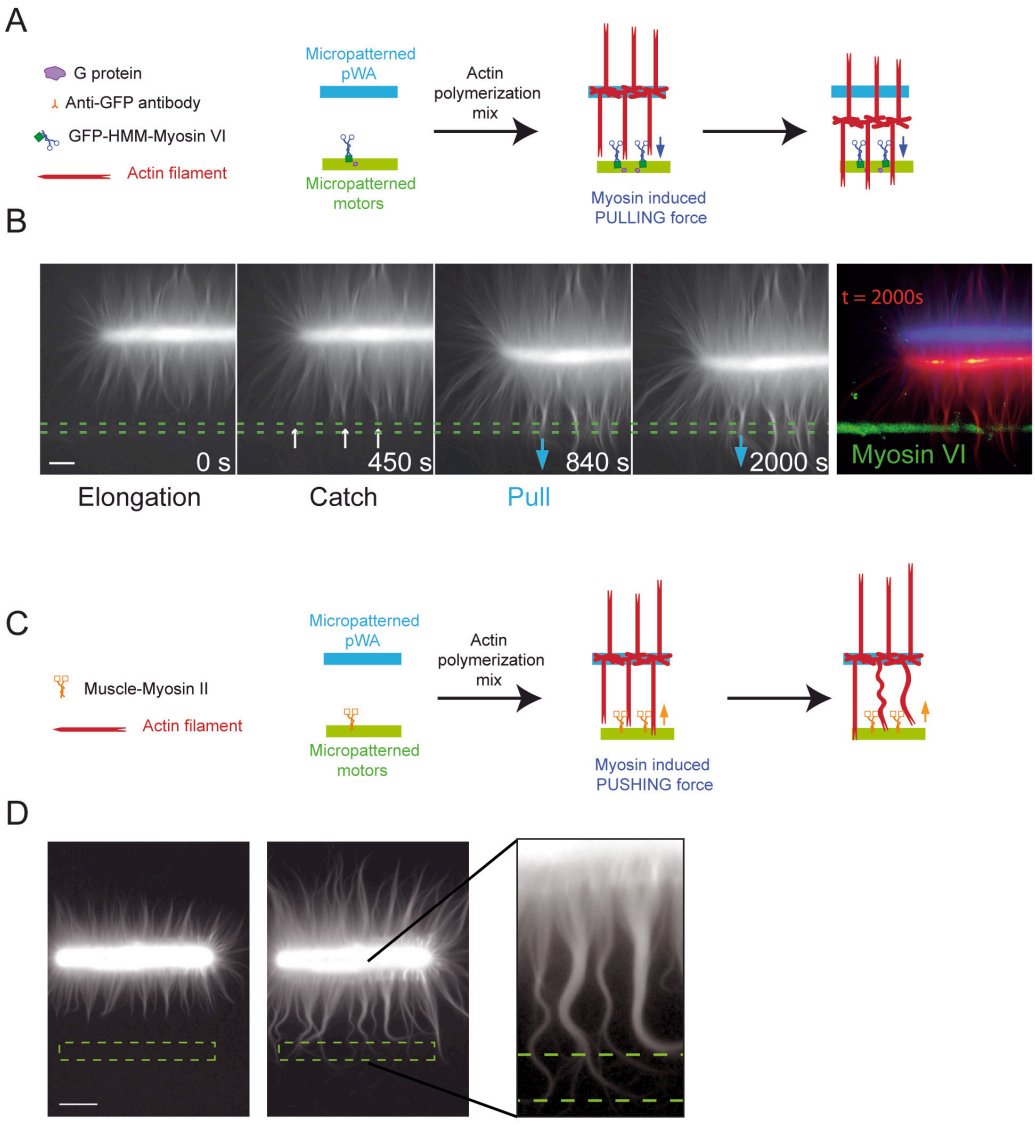

Fig. S5. Surface-tethered Myosin VI pulls on actin filaments and displaces actin networks.

(**A**) Schematic representation of the protocol of micro-patterned surface grafting dedicated to the study of fixed myosin VI-induced deformation of a simple patterned actin structure. (**B**) Time-lapse fluorescence microscopy of the elongation, tension and deformation of actin filaments nucleated on a micropatterned bar (actin monomers are labeled with Alexa-568) interacting with a patterned bar of grafted myosin VI (GFP tagged). The colored image is a combination of the acquisition of the myosin signal (green), as well as the first and last images of the actin fluorescence (respectively blue and red). Scale bar is 10 µm. (**C**) Schematic representation of the protocol of micro-

patterned surface grafting dedicated to the study of fixed myosin II-induced deformation of a simple patterned actin structure. (**D**) Time-lapse fluorescence microscopy of the elongation, tension and deformation of actin filaments nucleated on a micropatterned bar (actin monomers are labeled with Alexa-568) interacting with a patterned bar of grafted myosin II (not labeled). The zoomed image highlights the curvature of bundles interacting with the myosin II-coated bar. Scale bar is 10 μm.

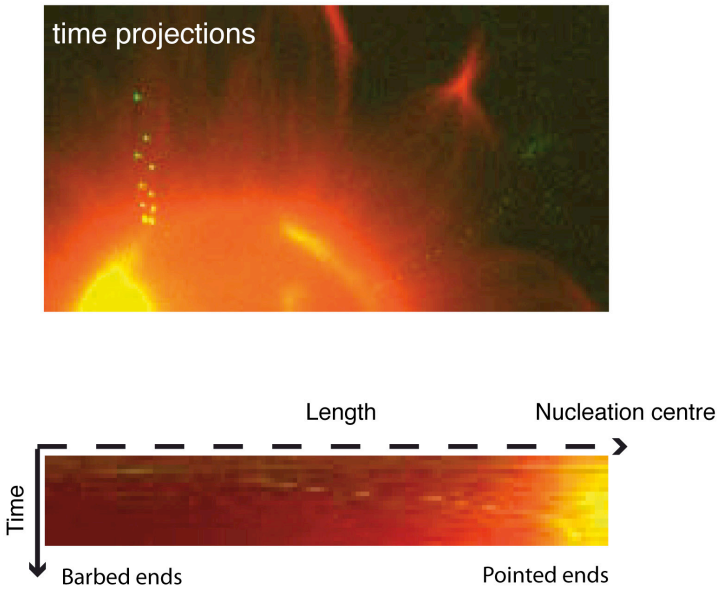

Fig. S6. Myosin VI walks on parallel filaments.

(**A**) Patches of GFP-HMM-myosin VI were monitored in time-lapse microscopy following their attachment to bundles of parallel filaments radiating out of a disc-shaped micropattern. The projection of all images acquired during the time sequence showed patches displacements. (**B**) A kimograph along one of these bundles revealed the displacement of GFP-HMM-myosin VI toward filament pointed ends.

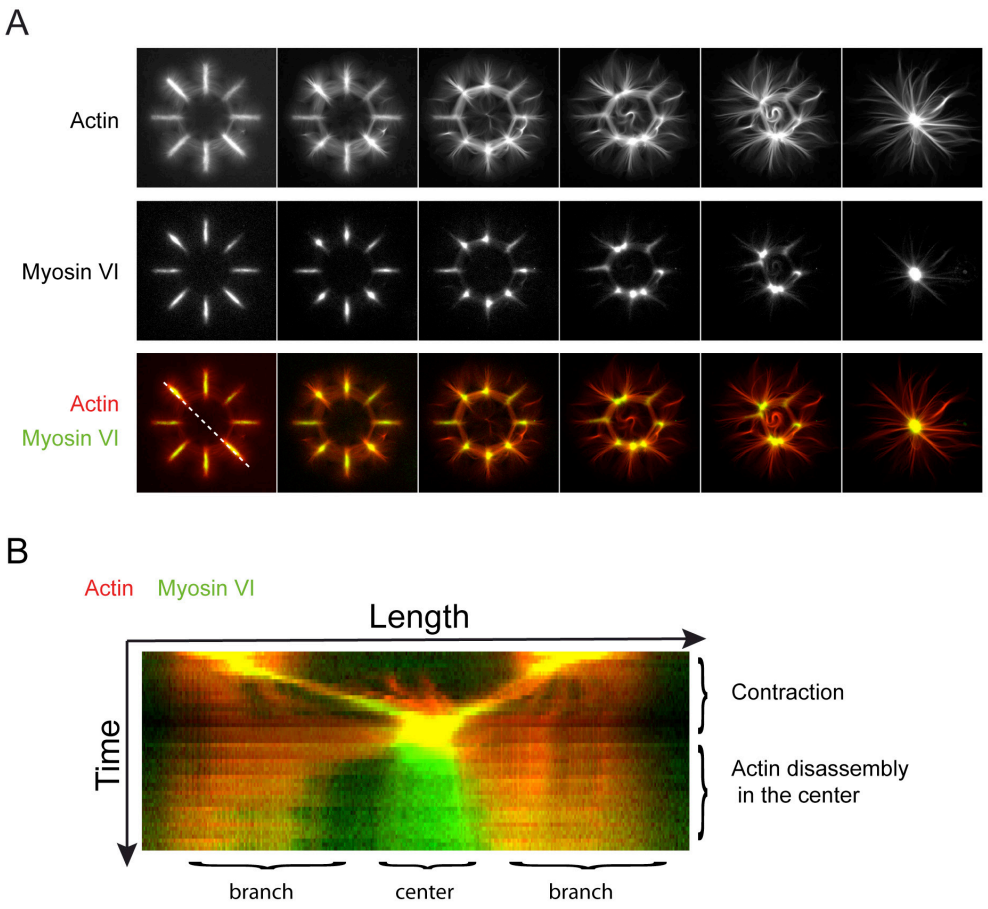

Fig. S7. Details of myosin-induced actin-network's contraction.

(**A**) Time-series of myosin-induced architecture selective contraction and disassembly, on an eight-branch actin nucleating radial array (actin, myosin and a color combine of both fluorescence are shown). (**B**) Double color kymograph along one branch of the array shown as the dotted line in A left bottom panel.

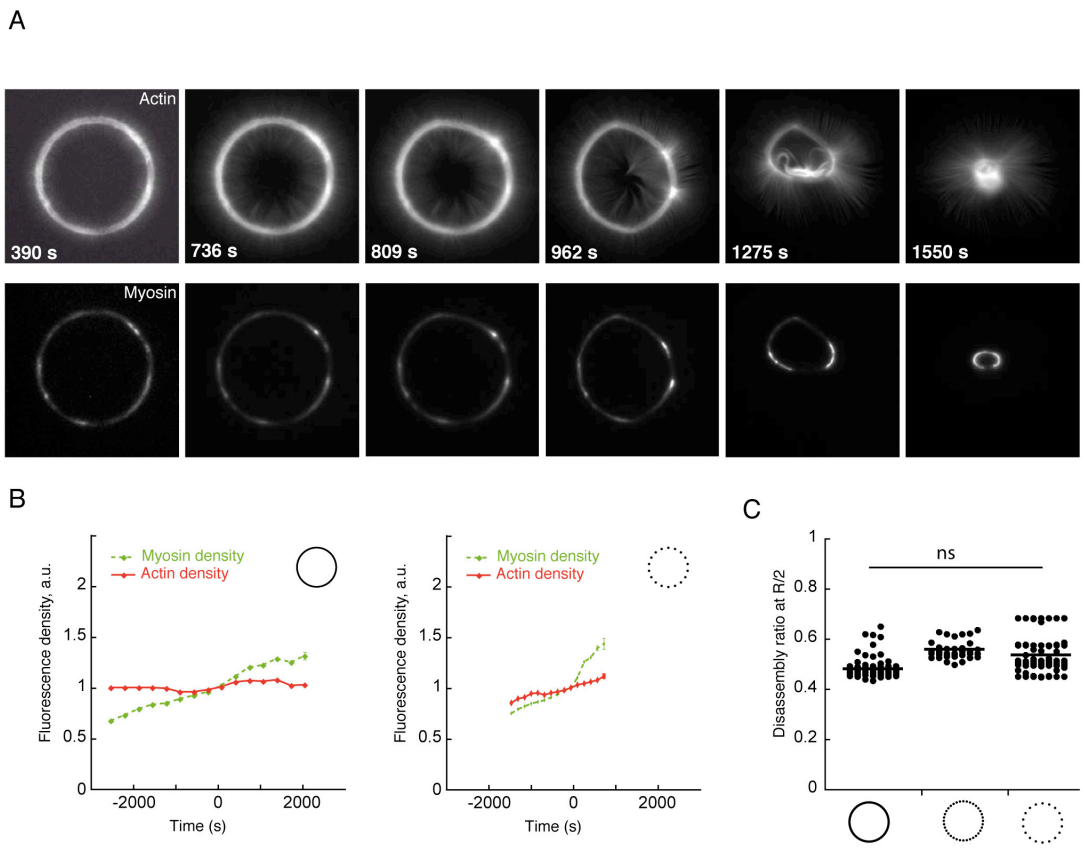

Fig. S8. Network density during contraction.

GFP-tagged myosins VI and Alexa-568-labeled actin monomers were used to observe network contraction on ring-shaped micropatterns. (**A**) Example of actin and myosin signals during actin network contraction on full ring. (**B**) Actin and myosin fluorescence intensities were measured during network contraction on full ring and dotted ring. Intensities were normalized with respect to ring length to reveal actin and myosin linear densities. Actin density is almost constant during deformation (after t = 0). Myosin density increased slowly with a constant slope before and after contraction on full ring. Errors bars represent standard error mean. (**C**) The disassembly of the actin network was estimated by dividing the total amount of actin when the radius was reduced to half its original size by its amount at the beginning of deformation. No significant differences could be measured between the different conditions leading to slow and fast contraction rates (see Fig. 3E). Statistical comparisons were Student T tests, ns= no significant difference: P>0.05.

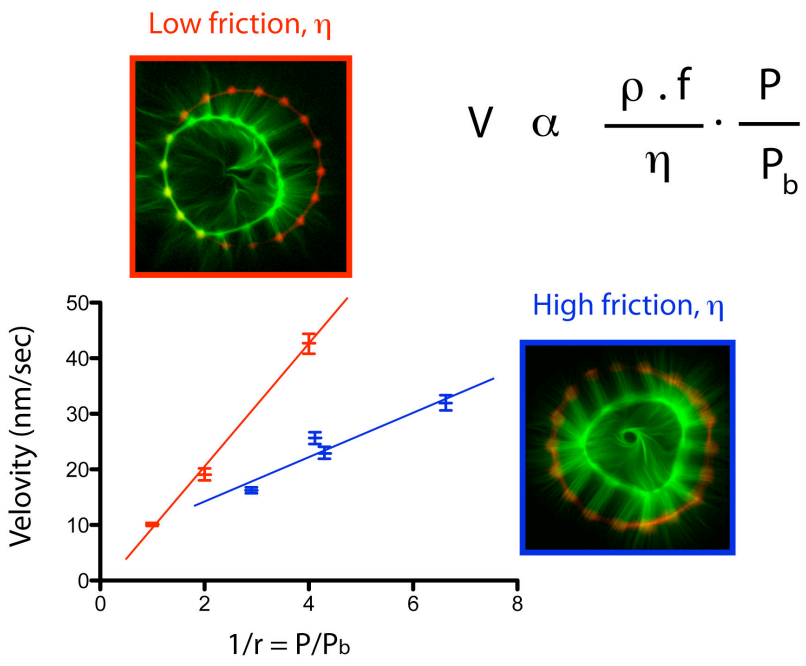

Fig. S9. Contraction velocity is proportional to nucleation ratio

Two sets of experiments were conducted with distinct micropatterning methods leading to different effective friction values during network contraction. The first set of experiments shown in Fig. 3 was performed with the deep UV-based micropatterning method on glass substrate (image with a red frame). The second set of experiments shown in Fig. 4 was performed with the pulsed UV-laser micropatterning method. In this case, the glass substrate is coated with a polystyrene layer, whose oxidation with the pulsed laser leads to a stronger attachment of nucleation regions and the formation of more numerous retraction fibers than with the deep-UV micropatterning of glass (see fibers connecting the contracted ring in the image with a blue frame). In both experiments the ring contraction velocity was proportional to the ratio P/Pb. Velocity values were reported from figures 3F and 4A. As expected from the model (Fig. 4B), a higher amount of retraction fibers leads to a higher effective friction coefficient η and thus to a reduced slope for velocity variations with respect to P/Pb.

Movie S1. Actin filaments growing on a pWA-coated bar. Actin polymerization is followed by TIRF microscopy. Left panel, actin filaments are branched on the patterned region and parallel outside this region. Right panel is a zoomed region (represented by the box in the left panel). Total elapsed time is 73 min and compressed to a 6-second QuickTime movie.

Movie S2. Myosin VI-induced actin meshwork contraction and disassembly. Montage of time-series of myosin VI-induced network contraction on a bar-shaped micropattern. Total elapsed time is ~ 2 hours and compressed to a 13-second QuickTime movie. An example of such network contraction on a bar-shaped micropattern is illustrated in Fig. 1A.

Movie S3. Myosin II-induced actin meshwork contraction and disassembly. Montage of time-series of myosin II-induced network contraction on a bar-shaped micropattern. Total elapsed time is 158 minutes and compressed to a 27-second QuickTime movie. An example of such network contraction on a bar-shaped micropattern is illustrated in Fig. 1B.

Movie S4. Myosin VI-induced contraction and disassembly of an actin network nucleated from a ring-shaped micropattern and crosslinked with 100 nM α-actinin. Total elapsed time is 3 hours 33 minutes compressed to a 7-second QuickTime movie.

Movie S5. Myosin VI-induced actin meshwork contraction and disassembly followed by TIRF microscopy. Same than movie S1 but in presence of myosin VI in the reaction mixture. Total elapsed time is 618 minutes and compressed to a 6-second QuickTime movie, that corresponds to the time-lapse series in Fig. S4.

Movie S6. Tension and/or deformation of cohesive actin network by myosins VI and II. Left, actin filaments nucleated from a micropatterned bar (4 μm width) coated with pWA, elongate and undergo tension and deformation as they interact with HMM-myosinVI spotted on an adjacent micropattern. Total elapsed time is ~33 min and compressed to a

4-second QuickTime movie, that corresponds to the time-lapse series in Fig. S5B. Right, actin filaments nucleated from a micropatterned bar (4 μm width) coated with pWA, elongate and undergo deformation as they interact with myosin II spotted on an adjacent micropattern. Total elapsed time is ~88 min and compressed to a 4-second QuickTime movie, that corresponds to the time-lapse series in Fig. S5D.

Movie S7. Left, dynamic organization of actin architectures assembled on an eight-branch nucleating radial array in absence of myosin. Total elapsed time is ~1h19 mn and compressed to a 5-second QuickTime movie, that corresponds to the time-lapse series in Fig. 2A. Right, regioselective myosin-induced contraction and disassembly of complex actin architecture. Kinetic of myosin-induced architecture selective contraction and disassembly, on an eight-branch actin nucleating radial array. As the denser entangled nucleating zones and the anti-parallel links between them rapidly contract and disassemble, the parallel bundles keep on elongating without perturbation. Total elapsed time is ~1h29 mn and compressed to a 5-second QuickTime movie, that corresponds to the time-lapse series in Fig. 2B.

Movie S8. Myosin-induced contraction of actin network nucleated on eight-branch nucleating radial arrays. Total elapsed time is 49 min and compressed to a 10-second QuickTime movie.

Movie S9. Myosin-induced contraction of actin network nucleated on full rings. The rings are 75 μm in diameter. Total elapsed time is 46 min and compressed to a 9-second QuickTime movie.

Movie S10. Comparison of myosin-induced contraction of actin network nucleated on a full (left) or dotted (right) ring. The rings are 75 μm in diameter. Total elapsed time is 19 min and compressed to a 10-second QuickTime movie, that corresponds to the time-lapse series in Fig.3.

Movie S11. Scalability of ring contraction. Rings of 50 microns (left) and 75 microns (right) in diameter constituted of 12 nucleation dots (top) or 18 nucleation dots (bottom) were contracted by HMM-myosin VI at different velocities (see Fig. 4A for measurements). Total elapsed time is 20 minutes and compressed to 11 seconds QuickTime movie.